D. Vinnikov, A. Chub, E. Liivik, R. Kosenko and O. Korkh

" Solar Optiverter—A Novel Hybrid Approach to the Photovoltaic Module Level Power Electronics "

IEEE Transactions on Industrial Electronics, vol. 66, no. 5,
pp. 3869-3880, May 2019.
doi: 10.1109/TIE.2018.2850036

Solar Optiverter—A Novel Hybrid Approach to the Photovoltaic Module Level Power Electronics

Dmitri Vinnikov, *Senior Member, IEEE*, Andrii Chub, *Member, IEEE*, Elizaveta Liivik, *Member, IEEE*, Roman Kosenko, *Student Member, IEEE*, and Oleksandr Korkh, *Student Member, IEEE*

***Abstract*—In this paper, the concept of an Optiverter is proposed as a novel class of photovoltaic (PV) module level power electronics systems. Functionally, the Optiverter is a hybrid technology that combines the ultrawide maximum power point tracking (MPPT) voltage window of the PV power optimizers with the direct ac connectivity and inherent safety of the PV microinverters. Thanks to the advanced multimode control with variable dc-link and the shade-tolerant MPPT algorithm, the proposed Optiverter ensures efficient energy harvest from the PV module in different shading scenarios. To justify the superiority of the concept, the performance of a 300 W prototype of the PV Optiverter is experimentally compared to that of the industrial microinverters in different operation conditions, including an extreme case with opaque shading of two out of three substrings of the PV module.**

***Index Terms*—Maximum power point tracking (MPPT), microinverter, module level power electronics, partial shading, efficiency, photovoltaic (PV) systems, power optimizer.**

I. Introduction

OVER the last decade, the photovoltaic (PV) module level power electronics (MLPE) has attracted increasing attention of the PV system operators and installers since it allows operation of each PV module in the maximum power point (MPP), thus ensuring the best possible energy yield from the PV installation [1]. Depending on the processed power, the PV MLPE systems can be broadly categorized as those with partial- or full-power conversion, from which the latter is more favorable due to better versatility and performance in different operating scenarios of the PV installation [2].

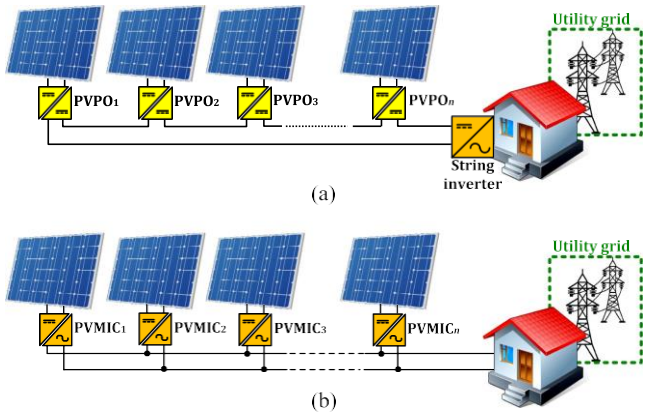

Fig. 1. Generalized schematics of MLPE-based grid-connected PV systems: with PVPOs (a) and with PVMICs (b).

Today's full-power MLPE systems are mostly represented by the PV power optimizers (PVPOs) and microinverters (PVMICs). The PVPO is an add-on component to the typical PV string installation, where the PV modules are connected in series, as shown in Fig. 1(a). Attached to or integrated in the junction box of a PV module, a PVPO is designed to increase the power yield of the module before it sends an optimized dc voltage to the string inverter. The PVPO is typically a nonisolated buck–boost dc–dc converter (NIBBC), which continuously adapts the current drawn from the PV module to maintain a fixed string voltage regardless of string characteristics and operating conditions of the PV modules [3]. The important advantage of the PVPOs is the ultrawide input voltage range; therefore, they can be paired with the vast majority of the PV modules, including high-power 72- and 96-cell modules and thin-film PV panels. Despite its overall simplicity, the series string installation with a PVPO still has several design constraints such as the minimal string length requirement of six to eight PV modules and impossibility of oversizing of the PVPO. Due to the small component count, the PVPOs typically feature efficiencies of over 98% and high reliability [4]. However, the string inverter needed for feeding PV power to the ac grid could potentially be a "bottleneck" of the PV installation

Manuscript received February 23, 2018; revised May 10, 2018 and June 5, 2018; accepted June 6, 2018. Date of publication July 3, 2018; date of current version December 28, 2018. This work was supported in part by the Ubik Solutions LLC and financed in part by the Estonian Centre of Excellence in Zero Energy and Resource Efficient Smart Buildings and Districts under Grant 2014-2020.4.01.15-0016 of the European Regional Development Fund and in part by the Estonian Research Council under Grant PUT1443. *(Corresponding author: Dmitri Vinnikov.)*

D. Vinnikov is with the Department of Electrical Power Engineering and Mechatronics, Tallinn University of Technology, 19086 Tallinn, Estonia, and also with the Ubik Solutions Ltd., 11911 Tallinn, Estonia (e-mail: dmitri.vinnikov@ttu.ee).

A. Chub, E. Liivik, and O. Korkh are with the Department of Electrical Power Engineering and Mechatronics, Tallinn University of Technology, 19086 Tallinn, Estonia (e-mail: andrii.chub@ttu.ee; liisa.liivik@ttu.ee; oleksandr.korkh@ttu.ee).

R. Kosenko is with the Ubik Solutions Ltd., 11911 Tallinn, Estonia (e-mail: roman@ubiksolutions.eu).

Color versions of one or more of the figures in this paper are available online at http://ieeexplore.ieee.org.

Digital Object Identifier 10.1109/TIE.2018.2850036

due to the single-point-of-failure problem. Another issue could be associated with risks of fire due to arcing on the high-voltage dc wires between the PV modules and the string inverter, which is typically located in the climate-controlled space. Therefore, extra safety features are required, including arc detection and fast safety disconnection of the PV installation.

In contrast to the PVPO, the PVMIC does not only maximize the energy harvest from the PV module but also converts the output voltage of the module to the grid compliant ac voltage. The PVMICs are connected in parallel at the grid side as shown in Fig. 1(b); therefore, the requirement for a minimal number of PV modules is not a constraint any more. This results in excellent flexibility of sizing since the PV installation can be easily scaled up and down by adding or removing PV modules with associated PVMICs. On the other hand, the PVMIC with its multistage power conversion and embedded control, protection and communication systems has a significantly increased component count, which penalizes their cost per watt and can have a negative impact on the power conversion efficiency. Another issue of the PVMIC is the long-term reliability since the increased number of components could potentially lead to higher failure rates, especially at the high cell temperatures, which can exceed 60 °C [5]. One of the main disadvantages of the PVMICs is the narrow maximum power point tracking (MPPT) voltage range, which is typically compromised by the tradeoff between the cost, efficiency, and reliability.

This paper introduces the concept called Optiverter (PVOPT) as a novel class of PV MPLE systems. Functionally, the PVOPT is a hybrid technology, which combines the ultrawide MPPT voltage range of the PVPOs with the direct ac connectivity and inherent safety of the PVMICs. In addition, it has the PV module level monitoring and safety cutoff, flexibility of installation, and PV power system sizing, which are important features of any MLPE system. First, the paper compares the state-of-the-art MLPE technologies and explains the essence of the proposed PVOPT technology. Next, the hardware and control system architectures of the PVOPT are presented, followed by the analysis of its advanced feature called shade-tolerant MPPT (ST-MPPT). To prove the concept, a 300 W PVOPT was assembled. Our test results are discussed in the experimental parts of the paper. Finally, the conclusions are drawn.

II. Comparison of State-of-the-Art MLPE Technologies

Fig. 2 shows several examples of the state-of-the-art MLPE topologies. The NIBBC shown in Fig. 2(a) is the most popular topology for PVPOs. The benefits are the small component count and overall simplicity of realization that help to solve such important issues of MLPE systems as cost per watt and reliability. Since the NIBBC has inherent buck–boost characteristics, the multimode control is usually implemented where, depending on the string current, the PVPO can feature one of the three modes of operation: buck, boost, and pass-through (PTM) [6]. This feature allows achieving an ultrawide range of input voltage and load regulation at high efficiency, which is one of the distinct benefits of the PVPOs over the PVMICs.

For the realization of PVMICs, the two basic approaches are mainly considered, which differ by the type of the dc-link and localization of the decoupling capacitor C_D. One of the most popular PVMIC topologies today is the interleaved flyback converters with an unfolding bridge shown in Fig. 2(b) [7]. Such configuration with a pseudo dc-link is often referred to as a single-stage PVMIC where the only way to implement the decoupling capacitor is to place it at the PV side [8]. Due to their relative simplicity, the single-stage PVMICs typically have more affordable price and efficiency than the multistage counterparts. In regard to the drawbacks, the localization of the decoupling capacitor at the low-voltage side results in a high capacitance values since the allowable voltage ripple must be typically kept below 5% in order to achieve the highest possible MPPT efficiency [9]. Depending on the operating power and system specifications, the required capacitance in several cases could exceed 10 mF, which influences negatively the power density and reliability of the PVMIC because of the bulky electrolytic capacitors typically used in the design.

For the multistage PVMIC design, the main power decoupling capacitor is placed at the high-voltage dc-link, as shown in Fig. 2(c) [10]. As compared to the PV-side decoupling where the voltage ripple should be limited to a very small value to maximize the MPPT efficiency, the dc-link decoupling allows for a higher dc-link voltage as well as a higher voltage ripple. According to (1), this leads to the progressive reduction of the decoupling capacitance since the voltage levels at the PV-side and HVdc-link side typically differ by more than 15 times

$$C_D = \frac{P}{2 \cdot \pi \cdot f_g \cdot V_D \cdot \Delta V_D} \tag{1}$$

where P is the operating power, f_g is the grid frequency, V_D and ΔV_D are, respectively, the operating voltage and the voltage ripple across the decoupling capacitor.

Table I shows the main specifications of the industrial MLPE systems. It can be seen that the PVPO has such important competitive advantages over the PVMIC as the ultrawide MPPT voltage window and high-rated power, which can drastically improve the energy yield of the PV system by minimizing the power losses associated with partial shading or power clipping effects. Furthermore, the PVPOs offer better versatility and PV module compatibility since the same model of the PVPO can be paired with different 60- and 72-cell modules. Contrary to that, the PVMICs are typically differentiated by the models compatible either with 60- or 72-cell PV modules.

In competition with the string inverters, the MLPE market today is mostly driven by the efficiency of the power conversion stage η_{CONV}; however, the MPP tracking efficiency also plays a crucial role since it strictly defines the power harvested from the PV module

$$P = P_{PV} \cdot \eta_{MPPT} \cdot \eta_{CONV} \tag{2}$$

where P_{PV} is the available power of the PV module, η_{CONV} is the ratio of the output and the input power of the converter ($\eta_{CONV} = P_{ac}/P_{dc}$), and η_{MPPT} is the ratio of the input power of the converter and available power of the PV module ($\eta_{MPPT} = P_{dc}/P_{PV}$). It is evident from Table I that in contrast to

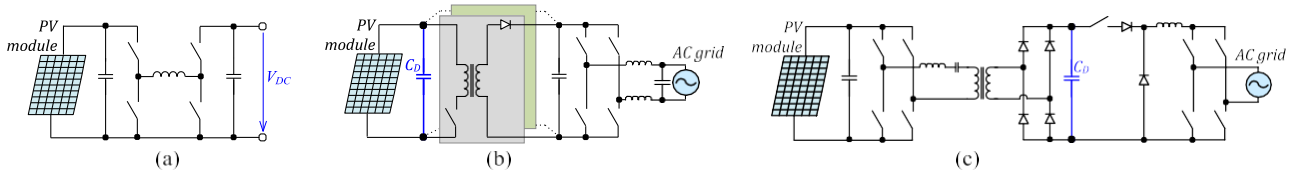

Fig. 2. Examples of industrial MLPE topologies: (a) NIBBC for PVPO, (b) interleaved flyback converters with unfolding bridge for PVMIC, and (c) resonant full-bridge dc–dc converter with single-buck inverter for PVMIC.

TABLE I
SPECIFICATIONS OF DIFFERENT MLPE SYSTEMS

MLPE technology	Power Optimizer (PVPO)	Microinverter (PVMIC)		Optiverter (PVOPT)
Model/type	*SolarEdge P370 [11]*	*Enphase M250 [12] (single-stage)*	*Enecsys 240-60-MP [13] (two-stage)*	*New proposed approach (two-stage)*
Topology	Fig. 2*a*	Fig. 2*b*	Fig. 2*c*	Fig. 5
Input voltage range	8…60 VDC	16…48 VDC	21…44 VDC	8…60 VDC
MPPT range	8…60 VDC	27…39 VDC	24…35 VDC	8…60 VDC
Minimum start-up voltage	8 V	22 V	22 V	8 V
Rated input power	370 W	250 W	250 W	300 W
Output voltage	≤60 VDC	230 VAC	230 VAC	230 VAC
Peak efficiency of power circuit	99.5%	96.5%	96.4%	96.2%
Peak MPPT efficiency	N.A.	99.4%	N.A.	99.5%
Minimum string length	8 units for 1-ph. system 16 units for 3-ph. system	1 unit	1 unit	1 unit
Type of PV module	60- and 72-cell PV modules	60-cell PV modules	60-cell PV modules	60- and 72-cell PV modules

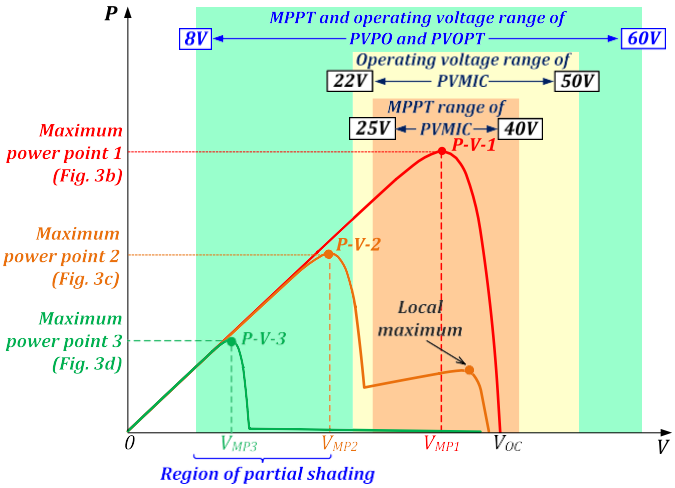

Fig. 3. Typical *P–V* curves of the PV module and MPPT voltage windows of different MLPE systems.

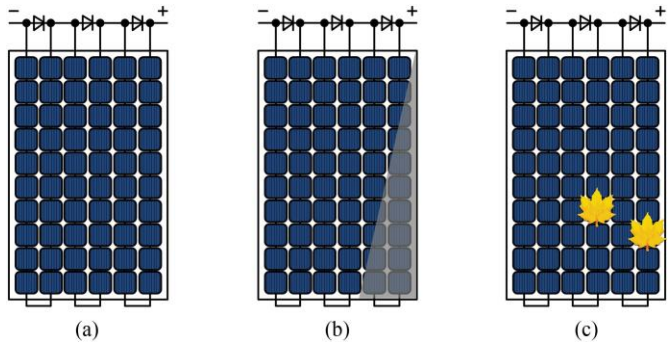

Fig. 4. Different shading scenarios of the PV module with reference to Fig. 3: (a) uniform irradiation of cells, (b) PSC with one shaded substring, and (c) opaque shading of two substrings.

the PVPOs, the PVMICs have a much narrower MPPT voltage window, which is often compromised by the design tradeoffs to achieve higher efficiency of the power conversion stage η_{CONV} at more affordable cost. As a result, the PVMICs are mainly able to track only the local power maximum similar to that indicated in the *P–V-1* curve in Fig. 3, i.e., in the conditions of uniform irradiation of cells in the PV module as shown in Fig. 4(a). However, in urban conditions, PV modules can often experience different partial shading effects, which could be caused by various obstructions like trees, roof top structures, and neighboring buildings as well as by soiling, i.e., deposition of dust, bird droppings, snow, etc. on the surface of the PV module. Such kind of partial shading results in different irradiation of the substrings of the PV module as shown in Fig. 4(b), which will lead to the appearance of two or three power maximums in the *P–V* curve of the module (e.g., *P–V-2* in Fig. 3). Because of a narrow MPPT window, the typical PVMIC in that case will typically stack at the local maximum, which will result in the progressive decrease of the MPPT efficiency (down to 35–40%) and partial shading power loss of up to two-thirds of the available power of the PV module.

The partial shading effect could also appear due to fallen leaves or bird droppings, which is known as opaque shading. In that case, the shaded substring(s) are bypassed by the integrated bypass diode(s), which causes a drop in the output voltage of the PV module. If two substrings are blocked by the leaves, as shown in Fig. 4(c), the PV module can potentially lose two-third of its output voltage (*P–V-3* in Fig. 3). In such scenario,

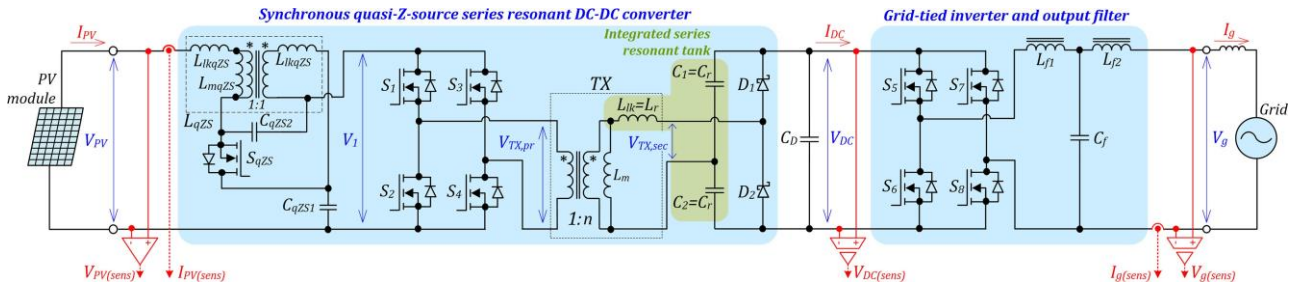

Fig. 5. Generalized power circuit diagram of the proposed PVOPT.

the PVMIC with the minimum start-up voltage of 22 V will not be able to identify the energy output of the PV module and will continue operating in a standby mode. Finally, the lower boundary of the MPPT voltage window of the PVMIC seriously compromises the energy yield from the PV module in partial shading conditions (PSC). According to Table I, the PVPO can start tracking the MPP from a voltage as low as 8 V, which enables the energy harvest from a severely shaded PV module.

III. PV Optiverter (PVOPT)

To fill the existing technology gap between the PVPO and the PVMIC a hybrid approach called Optiverter (PVOPT) is proposed as a novel class of PV MLPE systems. The PVOPT combines the ultrawide MPPT voltage range and shade-tolerant performance of the PVPOs with the direct ac connectivity and inherent safety of the PVMICs. Essentially, the concept of Optiverter proposed combines a wide-range buck–boost front-end dc–dc converter with highly efficient PTM and variable dc-link voltage control, a full-bridge grid-tied inverter, and the multimode control. Thanks to the advanced multimode control, the MPPT voltage window of the PVOPT is more than four times wider than that of the traditional PVMIC (see Table I). Furthermore, the minimum start-up voltage of the PVOPT was shifted down to 8 V, which ensures the energy harvest from the majority of 60- and 72-cell PV modules in different shading scenarios, including extreme opaque shading of two out of three substrings of the PV module.

A. Design of Power Conversion Stage

Generalized power circuit diagram of the proposed PVOPT is shown in Fig. 5. To enable the ultrawide MPPT voltage window with the possibility of tracking global maximums, the PVOPT was realized on the double-stage approach. The front-end quasi-Z-source series resonant dc–dc converter (qZSSRC) was justified as a superior solution for MLPE applications in [14]. In the given case, it is responsible for the MPPT and voltage matching between the PV module and the high-voltage dc-link. Generally, the front-end could be based on any other high-performance step-up dc–dc converter topology, allowing for input voltage and load regulation in a wide range, for example, a boost half-bridge dc–dc converter [4] or a hybrid series resonant and PWM boost converter [15]. However, as compared to its counterparts, owing to the inherent buck–boost characteristics and superior control flexibility, the qZSSRC features an unprecedented input voltage regulation capability and dc voltage gain range from 6.7 to 50 [16].

TABLE II
General Specifications of the Proposed PVOPT

Components	
S_1...S_4, S_{qZS}	Infineon BSC035N10NS5
D_1, D_2	Wolfspeed C3D02060E
S_5, S_6	Infineon IPB60R099C7
S_7, S_8	ROHM SCT2120AFC
L_{qZS}	L_{mqZS}=12 µH, L_{lkqZS}=0.6 µH, n=1
TX	L_m=1 mH, L_{lk}=24 µH, n=6
C_{qZS1}, C_{qZS2}	MLCC 26.4 µF (12 × KEMET C1210C225K1R in parallel)
C_1, C_2	Foil 43 nF (33 nF Epcos B32672Z6333K and 10 nF Vishay MKP1840310104)
C_D	El. cap. 150 µF Epcos B43501A6157M and foil 0.47 µF Epcos B32653A6474K
L_{f1}	2.6 mH
L_{f2}	1.8 mH
C_f	Foil 0.47 µF Epcos B32653A6474K
Control, driving and measurement	
Microcontroller	ST STM32F334
Drivers of MOSFETs	Analog Devices ADuM3223
Sw. freq. of qZSSRC	105 kHz
Sw. freq. of inverter	50 Hz for S_5, S_6 and 20 kHz for S_7, S_8
Dead-time of qZSSRC sw.	70 ns
Aux. power supply	TI LM46002 (Synchr. buck, 3.5…60 V)
Input side current sensor	Allegro ACS716KLATR-25CB-T
Input side voltage sensor	Resistive divider 1:20
Output side current sensor	Allegro ACS712ELCTR-05B-T
Output side voltage sensors	TI AMC1200-Q1

The design of the PVOPT is mainly based on the cost-performance tradeoff; therefore, special attention was paid to the integrity and hybridization of functions of the main components. For example, the transformer *TX* in the qZSSRC is not only providing the necessary voltage step-up and galvanic isolation but also supports the resonance and ensures the soft switching of the semiconductors. Thanks to the utilization of a series resonant tank formed by the leakage inductance L_{lk} of the transformer *TX* and capacitors C_1 and C_2 of the voltage doubler rectifier (VDR) and proper dimensioning of the magnetizing inductance and dead time, the qZSSRC is capable of achieving high efficiency through the full-ZCS of the VDR diodes over the entire operating range, and depending on the operating mode, ZVS and/or ZCS of the primary-side MOSFETs [17].

For the simplification purposes, the grid-tied inverter is based on the simple full-bridge topology with the combination of Si and SiC MOSFETs for the low-frequency (S_5, S_6) and high-frequency (S_7, S_8) legs, correspondingly. To attenuate

Fig. 6. Top view of the developed 300 W PVOPT.

the switching noise and create the sinusoidal output waveform, the *LCL* filter was employed at the output side of the PVOPT.

General specifications and top view of the developed 300 W PVOPT are presented in Table II and Fig. 6, correspondingly. As special attention was paid to the minimization of the manufacturing costs, the use of generic components was one of the main priorities of this project. For the unification purposes, all the magnetic components, including coupled inductor L_{qZS} and hybrid isolation transformer *TX*, were wound on the RM14 ferrite cores. Since the PVOPT utilizes only the natural convection cooling, specially optimized thermal pads and vias were employed on the printed circuit board (PCB) to move the heat from the parts into the core layers, thus eliminating the hotspots.

B. Advanced Multimode Control With Variable DC-link

The front-end qZSSRC is essentially the buck–boost converter with three possible operation modes [14], [17].

1) Pass-through mode (PTM): the qZSSRC operates as the series-resonant converter (SRC) in the dc transformer mode. The input and the output voltages of the qZSSRC are tightly coupled. The normalized dc voltage gain is unity, and voltage step-up is defined by the transformer turns ratio only:

$$tt_{PTM} = \frac{V_{DC}}{2 \cdot n \cdot V_{PV}} = 1. \tag{3}$$

As a result, the front-end qZSSRC transfers the PV module voltage from the input to the output with a fixed gain. The qZSSRC is modulated with a duty cycle of nearly 0.5 and frequency slightly below the resonance frequency of the resonant tank to achieve half-cycle discontinuous-conduction-mode (HC-DCM) when the resonance process is ended before switching the transistors [18]. This modulation results in robust zero voltage switching (ZVS), since the parasitic capacitance of the MOSFETs is recharged with the load-independent magnetizing current during the dead-time [19]. The dc voltage gain of the qZSSRC is virtually insensitive to the difference between the switching and the resonant frequencies due to the resonant tank quality factor much below unity [20], [21].

There are two degrees of freedom in the control of the PVOPT: dc voltage gain of the front-end converter and modulation index of the grid-tied inverter. In the PTM, the former is fixed and, consequently, the grid-side inverter has to handle both the MPPT and grid current control.

2) Buck mode: operation of the qZSSRC in the buck mode is similar to that of the traditional SRC with phase-shift modulation control at the resonant frequency and discontinuous resonant current. The latter is due to small leakage inductance values inherent to the conventional transformers, which results in the quality factor Q 1 in the whole operating range. The normalized dc voltage gain depends on the phase shift angle ϕ and the quality factor Q [26]:

$$tt_{buck(DCM)} = \frac{V_{DC}}{2 \cdot n \cdot V_{PV}} = 0.5 \cdot \left(A \cdot B + \sqrt{B^2 \cdot A^2 + A \frac{8}{\pi \cdot Q}} \right)$$

$$\text{where } B = \frac{2}{\pi \cdot Q} \left(1 - \cos \left(\frac{\varphi}{180} \pi \right) \right)$$

$$A = 0.5 - 0.5 \cdot \cos \left(\frac{\varphi}{180} \pi \right)$$

$$\text{and } Q = \frac{8\pi \cdot f_{SW} \cdot L_{lk} \cdot P_{DC}}{V_{DC}^2}. \tag{4}$$

3) Boost mode: the voltage step-up is controlled by shoot-through pulsewidth modulation implemented as a symmetrical overlap of active states [14]. Among the numerous methods of the shoot-through generation [22]–[25], this one provides the best utilization of the transformer and the lowest switching losses. The normalized dc voltage gain of the qZSSRC depends on the shoot-through duty cycle D_{ST} [14]:

$$tt_{boost} = \frac{V_{DC}}{2 \cdot n \cdot V_{PV}} = \frac{1}{(1 - 2 \cdot D_{ST})}. \tag{5}$$

The conventional multimode control described in [14] results in the qZSSRC operating in the PTM only at the particular voltage where (3) holds true for the fixed dc-link voltage. However, the PTM corresponds to the peak efficiency, and thus the qZSSRC cannot deliver high performance within the range of probable maximum power points of a PV module.

It is not necessary for the grid-tied inverter to have fixed dc-link voltage. Hence, the qZSSRC control with variable dc-link voltage could be implemented to cover the voltage range that overlaps with the voltage ranges of probable MPPs of 60- and 72-cell Silicone (Si) PV modules, as shown in Fig. 7. The lower bound of the PTM range is defined by the peak grid voltage $V_{g(pk)}$ with an assumption that the dc-link voltage is 10 V above that, which is expressed as follows:

$$V_{PV1} = \frac{V_{g(pk)} + 10}{2 \cdot n}. \tag{6}$$

The grid rms voltage is usually within the range of 207 V to 253 V, which results in possible variations of the minimum dc-link voltage $V_{DC(min)}$ from 305 V to 370 V. For the rated

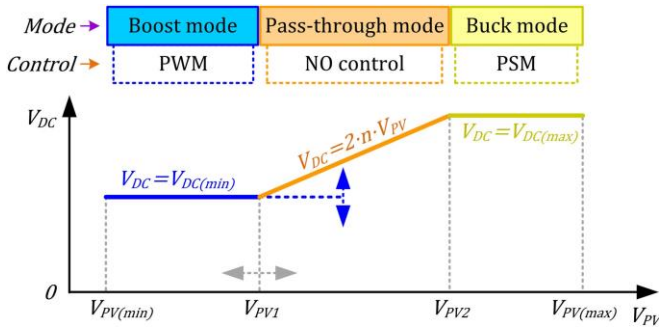

Fig. 7. Sketch of the proposed variable dc-link voltage control enabling efficiency optimization in the most probable range of the input voltages.

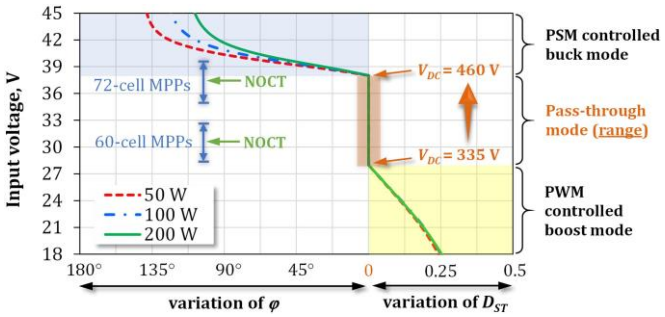

Fig. 8. Experimental control characteristic of the front-end qZSSRC operating with the variable dc-link voltage.

grid voltage of 230 V, this voltage equals $V_{DC(min)}$ = 335 V. The upper bound of the PTM is limited by the voltage rating of the dc-link capacitor. Considering the existing technology of electrolytic capacitors, the capacitor rated voltage of 500 V could be recommended. In this study, it is assumed that $V_{DC(max)}$ = 460 V, which results in a safety margin of 40 V:

$$V_{PV2} = \frac{V_{DC(max)}}{2 \cdot n}. \quad (7)$$

In the given case, the PTM is active between V_{PV1} = 28 V and V_{PV2} = 38 V for the nominal grid rms voltage of 230 V. The control characteristic of the qZSSRC are shown in Fig. 8 for the nominal grid voltage features considerable PTM range owing to the proposed advanced multimode control with variable dc-link voltage. The regulation range is more than 30% wider when compared to that with the fixed dc-link voltage. Remarkably, the PTM overlaps with the ranges of the most probable MPPs of 60- and 72-cell Si PV modules for the temperature variations between 30 °C and 60 °C. This includes the standard normal operating cell temperature (NOCT) of 45 °C. The MPPs outside the PTM correspond to either low or high temperatures rarely observed in practice.

A simple full-bridge inverter is used at the grid side. The asymmetrical unipolar PWM [27] is used in the inverter stage. It features only low-frequency common mode voltage, resulting in virtually no leakage current. During the positive half-cycle of the grid voltage, S_5 and the body diode of S_6 turn on alternately, and S_8 is turned ON for half of the grid period. During the negative half-cycle, S_6 and the body diode of S_5 turn on alternately, and S_7 is turned ON. The *LCL*-filter designed according to the methodology in [28] was used. The isolation transformer is an effective barrier to leakage currents due to low interwinding capacitance and, therefore, the leakage current is not a concern in galvanically isolated microinverters [1], [29]. The grid-tied inverter modulation renders the leakage current impossible.

C. Experimental Evaluation of the Optiverter

First, the PVOPT was tested with a solar array simulator (SAS) Agilent E4360A, emulating nominal operating conditions of 60-cell Si PV module JinkoSolar JKM300M-60 that is one of the leading products at the residential PV market. Current and voltage signals were measured by the oscilloscope Tektronix DPO7254, the current probe TCP0030A and the differential voltage probes P5205A. As shown in Fig. 9, the PVOPT features low input current and voltage ripple, and low grid current total harmonic distortion of 2.6% despite the presence of the fifth harmonic in the grid voltage. The current drawn by the grid-tied inverter from the dc-link (I_{DC}) is shifted in respect to the ac-component of the dc-link voltage, as could be expected for the single-phase system.

Electromagnetic compatibility was tested using a test receiver Rohde & Schwarz ESPI3. First, the conducted emission was measured with a line impedance stabilization network Schaffner MN2050D. The obtained result shown in Fig. 10(a) meets the requirements of the EN61000-6-3 standard. Next, radiated emission was tested with a converter in an extruded aluminum casing with plastic covers on two sides. Measurements were performed in a special chamber by means of a 30 dB preamplifier coupled with an antenna Schaffner CBL6112D directed toward one of the plastic covers. The test results shown in Fig. 10(b) meet the requirements of the EN55022 standard.

The California Energy Commission (CEC) weighted efficiency η_{CEC} was used for benchmarking. It is calculated as follows: $\eta_{CEC} = 0.04 \cdot \eta_{10\%} + 0.05 \cdot \eta_{20\%} + 0.12 \cdot \eta_{30\%} + 0.21 \cdot \eta_{50\%} + 0.53 \cdot \eta_{75\%} + 0.05 \cdot \eta_{100\%}$, where $\eta_{10\%}$, $\eta_{20\%}$, $\eta_{30\%}$, $\eta_{50\%}$, $\eta_{75\%}$, and $\eta_{100\%}$ are the efficiency values measured at 10%, 20%, 30%, 50%, 75% and 100% of the rated power, correspondingly [30]. A Yokogawa WT1800 was used in efficiency measurements.

The efficiency of the PVOPT was tested within the whole operating range according to a special power test profile (blue dash line in Fig. 11) that was proposed in [14] as a tool for performance assessment of wide-range MLPE dc–dc converters. This profile takes into account maximum input current range (left slope), maximum power range (V_{PV} from 28 V to 38 V), and start-up range (right slope); it envelopes averaged operating range of 60- and 72-cell Si-based PV modules that are common in residential PV systems. It is shown in Fig. 11 along with the measured efficiency at the fixed and variable dc-link voltage. The advanced multimode control with variable dc-link voltage improves the PVOPT efficiency in the whole operating range. At the fixed dc-link voltage, the highly efficient PTM is achieved only at V_{PV} = 33 V, while efficiency is decreasing when the operating voltage moves in either direction from this point of the maximum efficiency.

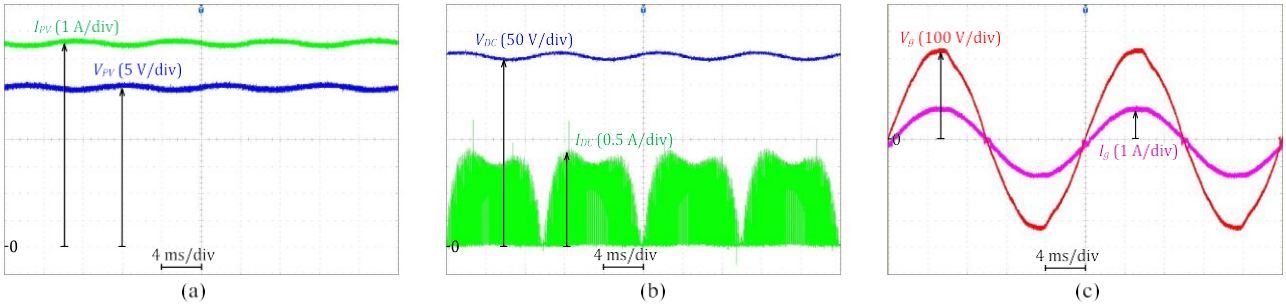

Fig. 9. Voltage and current waveforms of the Optiverter operating with JinkoSolar JKM300M-60 PV module under uniform irradiance of 800 W/m^2 and nominal cell temperature of 45 °C: (a) input voltage and current, (b) dc-link voltage and current, and (c) grid voltage and current.

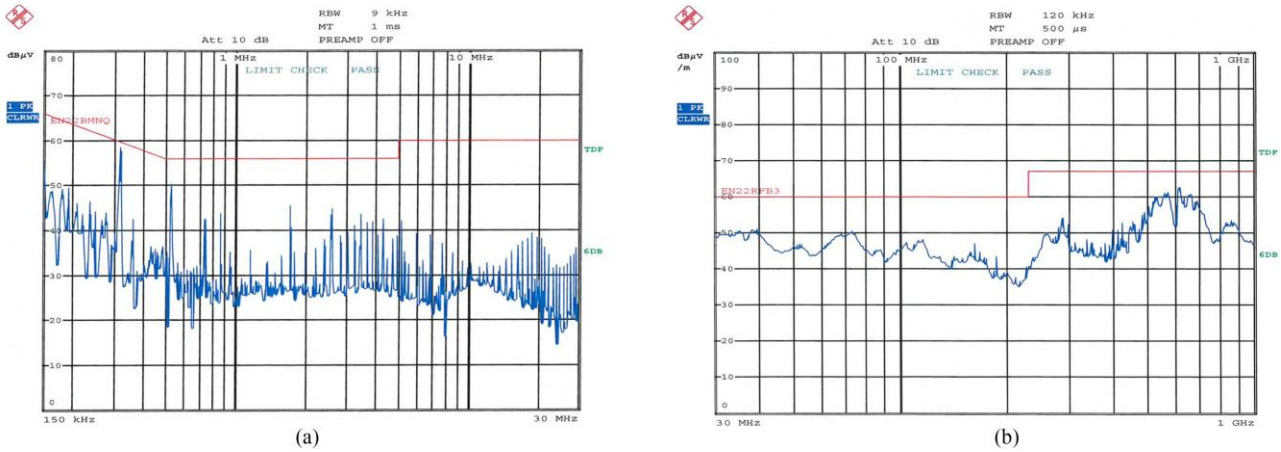

Fig. 10. Electromagnetic compatibility test results: (a) conducted emission in the range of 0.15 MHz to 30 MHz and (b) radiated emission in the range of 30 MHz to 1000 MHz.

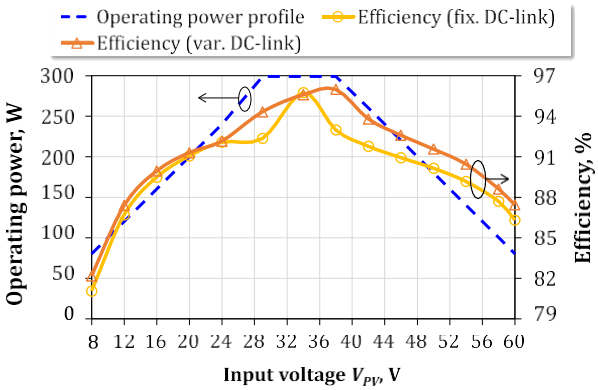

Fig. 11. Comparison of the measured efficiency for the variable and fixed dc-link voltage control and operating power profile used.

Efficiency of the PVOPT was measured over the power range of 10% to 100% at three voltages, taking into account auxiliary power supply consumption in order to calculate weighted efficiency, as shown in Fig. 12(a). The efficiency of the PVOPT is the same for both control methods at the point of V_{PV} = 33 V. At the fixed dc-link voltage, the curve for V_{PV} = 28 V (blue dash line with round markers) corresponds to the boost mode of the qZSSRC, while the curve for V_{PV} = 38 V (green dash line with triangular markers) corresponds to the buck mode of the qZSSRC. Efficiency in those modes is lower than in case of the PTM at V_{PV} = 33 V (red solid line with square markers). The efficiency of the front-end dc–dc stage operating with the variable dc-link voltage was measured separately, as shown in Fig. 12(b). It follows from Fig. 12 that except the point V_{PV} = 33 V, the PVOPT features up to 3.5% higher CEC weighted efficiency with the advanced multimode control.

It should be noticed that the efficiency of the PVOPT is limited due to design tradeoffs required to achieve a wide regulation range. However, more competitive efficiency values could be gained by the implementation of a cycle skipping modulation in the front-end dc–dc stage [14], [31]. With the different number of cycles skipped after an active cycle, the CEC weighted efficiency could be enhanced to 95.3% (blue line in Fig. 13), which will bring the PVOPT to the level of the market-leading 250 W single-stage PVMIC evaluated at the same input voltage (green dash line in Fig. 13). The light-load efficiency of the PVOPT could be also improved with the cycle skipping in the grid-tied inverter stage [32]. In addition, a low-cost reconfigurable rectifier can improve the qZSSRC efficiency by up to 8% in the PSC range [16]. Hence, the PVOPT efficiency can be improved up to the level that makes it competitive alternative to the commercial PVMICs, while it enables efficient energy harvest under partial or opaque shading conditions, which are not available with the existing commercial and research PVMICs.

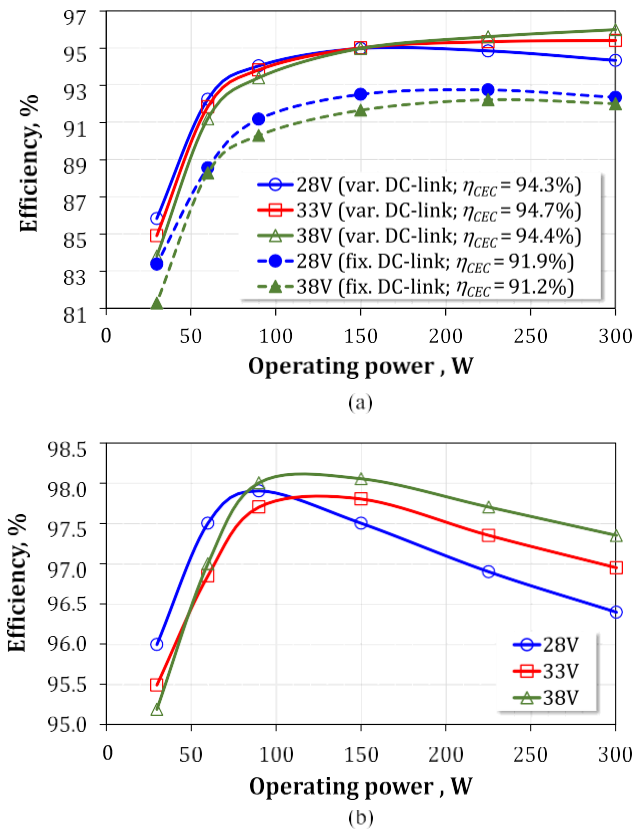

Fig. 12. Experimental efficiency: (a) the overall converter efficiency (η_{CONV}) and weighted efficiency values measured at different input voltages with variable and fixed dc-link voltage, taking into account auxiliary supply consumptions; and (b) efficiency of the front-end dc–dc converter operating with variable dc-link voltage.

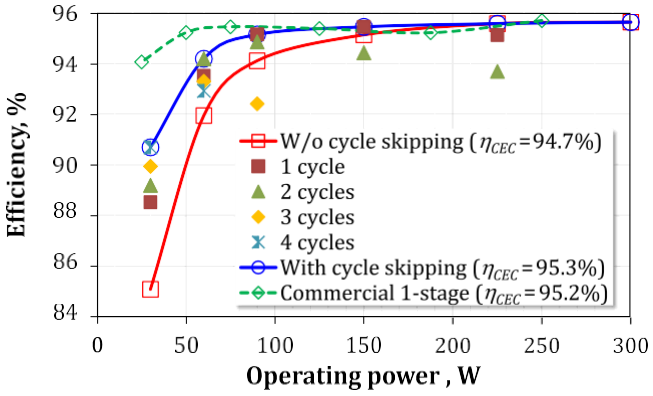

Fig. 13. Experimental efficiency of PVOPT at V_{PV} = 33 V: without cycle skipping, with a different number of skipped cycles in the dc–dc stage modulation, resulting envelope efficiency curve, and efficiency curve of a commercial single-stage PVMIC based on the topology from Fig. 2(b).

IV. Shade-Tolerant Maximum Power Point Tracking

The control system of the PVOPT shown in Fig. 14(a) contains two main proportional integral (PI) controllers: one for the qZSSRC (PI_1) and the other for the grid-tied inverter (PI_2). Positive output of PI_1 activates the boost mode, the negative output is used for the buck mode. The grid current tracking is based on the proportional resonant (PR) controller and selective

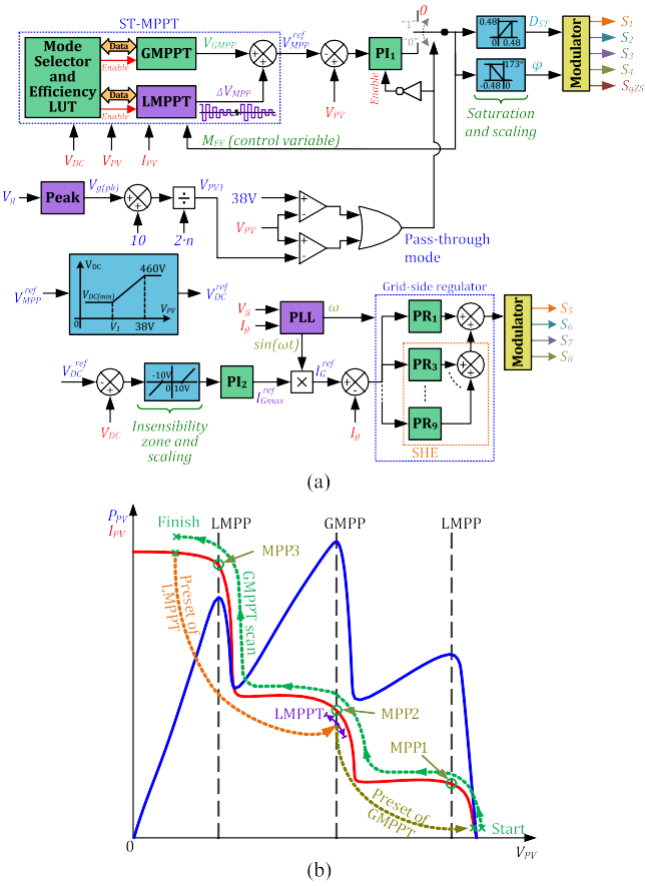

Fig. 14. (a) Simplified sketch of the PVOPT control system and (b) ST-MPPT implementation.

harmonic elimination (SHE) block comprising several PR controllers. The controller PR_1 is used to force the grid current I_g to follow the reference current (I_g^{ref}). The SHE is a part of the grid-side regulator that eliminates the odd harmonics, while a single PR controller is required for each harmonic. In the given case, controllers PR_3, PR_5, PR_7, and PR_9 are used to eliminate 3rd, 5th, 7th, and 9th harmonics, respectively. The PI controller PI_2 defines the amplitude of the reference grid current (I_g^{ref}), as shown in Fig. 14(a). During the PTM in the qZSSRC, MPPT is performed by the controller PI_2, while in the other two modes, both of the PI controllers are used for that.

A. Description of the ST-MPPT Algorithm

The PVOPT is superior to the PVMICs in partial shading and opaque shading conditions due to the implementation of the shade tolerant MPPT (ST-MPPT). From Fig. 14(b), it could be appreciated that the ST-MPPT consists of global MPPT (GMPPT) and local MPPT (LMPPT). This sketch preserves the essence of 60- and 72-cell Si PV modules that have three sub-strings and consequently, three integrated bypass diodes. The GMPPT is based on the *P–V* curve scanning that results in the identification of the MPPs: local (LMPPs) and the global one (GMPP). Next, the control system presets the control variables to obtain the operating point near the GMPP and activates the

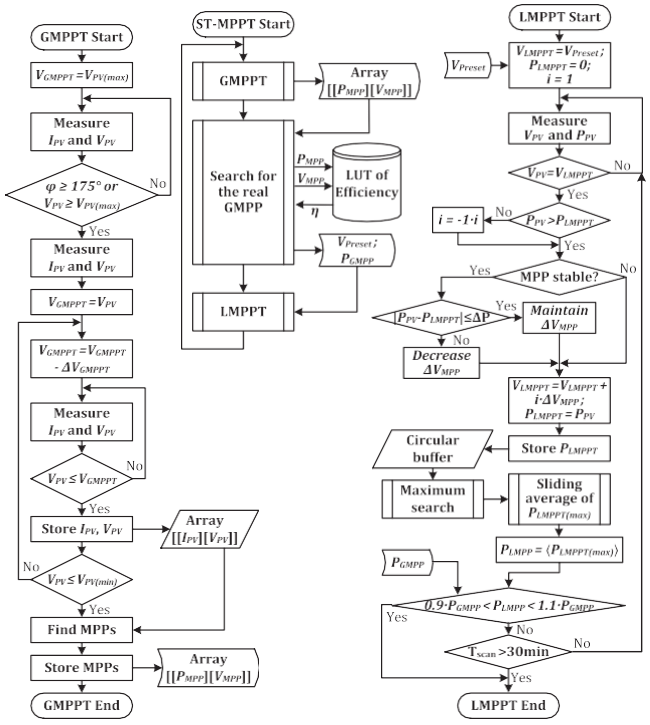

Fig. 15. Workflow of the ST-MPPT routine.

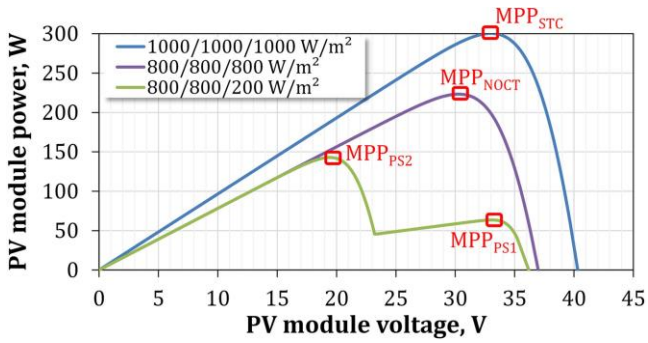

Fig. 16. *P–V* profiles of JKM300M-60 PV module: under STCs (MPP_{STC}), under NOCT of 45 °C and uniform irradiance of 800 W/m^2 (MPP_{NOCT}), and under partial shading of one substring down to an irradiance of 200 W/m^2 ($MPP_{PS\,1}$ and $MPP_{PS\,2}$).

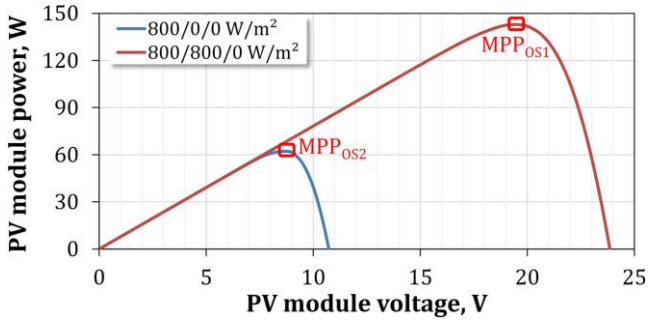

Fig. 17. *P–V* profiles of JKM300M-60 PV module: under NOCT of 45 °C and opaque shading of a single ($MPP_{OS\,1}$) and two substrings (MPP_{OS2}).

LMPPT that performs the perturbation of the operating point with variables steps to maximize the MPPT efficiency η_{MPPT}.

The workflow of the ST-MPPT is presented in Fig. 15. The ST-MPPT defines the reference PV module voltage, while the control system from Fig. 14(a) ensures that the PVOPT is reaching this point. The GMPPT rescanning is performed if the PV power changes by more than 10%, which is an evidence of changed operating conditions, or elapse of 30 min. It starts from the preset of the qZSSRC. The preset ends when either maximum input voltage or maximum voltage step-down ratio of the qZSSRC is achieved. Then, the reference voltage of the PV module is gradually decreased until it reaches the minimum allowed value. The data stored during the GMPPT are postprocessed by the application of the PVOPT efficiency taken from the predefined look-up table. This enables PVOPT operation in MPP with higher voltage and higher output power when there are two MPPs of close power at two different voltages. Operation at higher voltage, i.e., higher efficiency, would result in fewer thermal cycles corrupting the reliability.

B. Experimental Verification of ST-MPPT Performance

In this subsection, the PVOPT is compared to the two commercial PVMICs: market leading single-stage PVMIC based on the topology from Fig. 2(b) and commercial two-stage PVMIC based on the topology from Fig. 2(c). Further experimental studies harness different operating scenarios of a JinkoSolar JKM300M-60 PV module. *P–V* profiles for unshaded and partially shaded conditions are shown in Fig. 16, while Fig. 17 presents those for the opaque shading. More insight on irradiation of each of the three substrings and operating temperature are shown in Table III. These power profiles were tabulated using the PV module model in MATLAB Simulink that takes into account three integrated bypass diodes and is based on the two-diode model of a PV cell [33]. These profiles were emulated by a SAS Agilent E4360A that was also used to measure the static MPPT efficiency (η_{MPPT}).

The PVOPT and two PVMICs were tested with the *P–V* profile from Fig. 16, corresponding to the PSC. It could be appreciated from Fig. 18 that the commercial PVMICs are capable of tracking only the first local MPP ($MPP_{PS\,1}$), while the PVOPT perform scanning of the whole PV curve and continued operation in the real GMPP ($MPP_{PS\,2}$). The variable dc-link voltage between 335 V and 430 V corresponds to the qZSSRC operating in the PTM during the GMPPT scanning. Hence, the PVOPT has outperformed competitors in the PSC.

C. Comparative Analysis of MPPT Efficiency

The PVOPT was compared to commercial PVMIC using the overall PV power conversion efficiency: $\eta_{PV} = \eta_{CONV}\,\eta_{MPPT}$. This approach corresponds to the definitions from the standard EN 50530:2010 "Overall efficiency of photovoltaic inverters." Three samples were tested with five possible scenarios from Figs. 16 and 17. The test results are presented in Table III. Measurements with the *P–V* profile corresponding to the standard test conditions (STCs) were shown to explain the power clipping problem. It appears when the available PV power is higher than the power rating of a PVMIC; consequently, the latter limits the

TABLE III
BENCHMARKING RESULTS OF COMMERCIAL PVMICS AND THE OPTIVERTER UNDER DIFFERENT PRACTICAL OPERATING CONDITIONS

P-V profile (irradiance and temperature of 3 substrings)	*Commercial single-stage PVMIC*				*Commercial two-stage PVMIC*				*Optiverter*			
	MPP	η_{MPPT}, %	η_{CONV}, %	η_{PV}, %	MPP	η_{MPPT}, %	η_{CONV}, %	η_{PV}, %	MPP	η_{MPPT}, %	η_{CONV}, %	η_{PV}, %
STC (Fig. 16): 1000/1000/1000 W/m^2; 25°C	MPP_{STC}	85.6*	95.2	81.5	MPP_{STC}	74.7*	95.3	71.2	MPP_{STC}	99.3	95.65	**95**
NOCT (Fig. 16): 800/800/800 W/m^2; 45°C	MPP_{NOCT}	99.2	95.2	94.4	MPP_{NOCT}	99.1	95.8	**94.9**	MPP_{NOCT}	99.5	94.1	93.6
PSC (Fig. 16): 800/800/200 W/m^2; 45°C	MPP_{PS1}	44.5	95.4	42.5	MPP_{PS2}	44.3	92.7	41.1	MPP_{PS2}	99.3	91.6	**91**
Opaque shading (Fig. 17): 800/800/0 W/m^2; 45°C	MPP_{OS1}	99.5	95	**94.5**	MPP_{OS1}	40.1**	94.7	34	MPP_{OS1}	99.4	91.5	91
Severe opaque shading (Fig. 17): 800/0/0 W/m^2; 45°C	Standby mode				Standby mode				MPP_{OS2}	99.2	79	**78.4**

*Power clipping appears; **PVMIC stopped MPPT at its minimum allowed voltage of roughly 23 V.
Bold face is used to identify the best performing device under each test condition.

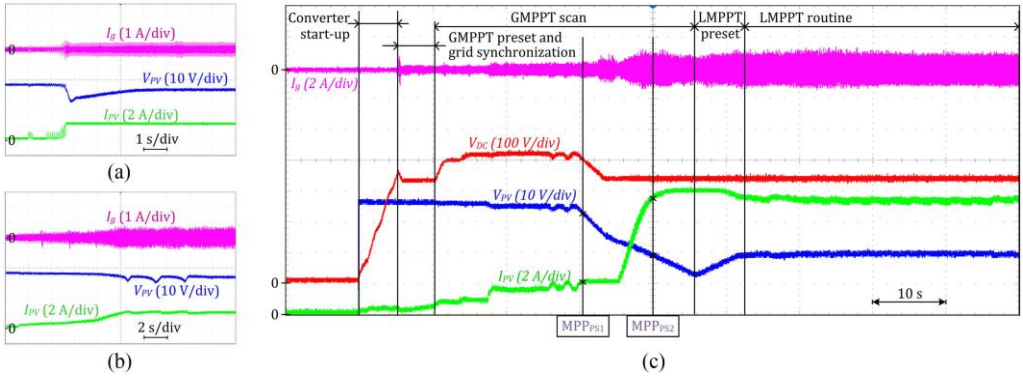

Fig. 18. MPPT during start-up of the (a) single-stage and (b) two-stage commercial PVMICs, and (c) start-up and ST-MPPT routine of the PVOPT.

input power. Since the nameplate power of modern PV modules is rising gradually, the MLPE converters should be rated above that of the modern PV modules to be compatible with the emerging PV modules.

Both of the commercial PVMICs failed to deliver high energy yield under the PSC. Under the opaque shading of a single substring, only the single-stage PVMIC was able to show good performance, while in the case of two blocked substrings, both failed to deliver any power. Moreover, voltage clipping was observed for the two-stage PVMIC. Overall, the PVOPT delivers good performance in unshaded conditions slightly behind the commercial PVMICs, while its performance is unparalleled under partial and opaque shading. Power conversion efficiency can be further improved if the optimization methods, like cycle skipping modulation discussed above, are properly utilized.

V. CONCLUSION

In this paper, the novel concept of the PVOPT with an ultrawide input voltage range was proposed and justified as a shade-tolerant solution for residential and small commercial PV installations, which is compatible with a wide variety of modern residential PV modules. It outperforms conventional microinverters under partial shading due to the implementation of the shade tolerant MPPT and can deliver power under severe opaque shading conditions, when the microinverters fail to capture any power due to their limited input voltage regulation range. Moreover, it is compatible with emerging high-power PV modules due to increased power rating for avoiding the power clipping. These features result from the application of the galvanically isolated ultrawide range buck–boost dc–dc converter and the novel control principle with the variable dc-link voltage that optimizes efficiency in the most probable input voltage operating range. This enables the shade tolerant MPPT through *P–V* curve scanning. Hence, the PVOPT can be used as a versatile solution for residential and small commercial PV installations. Using single stock keeping unit for different PV modules decreases installation and shipping costs as well as staff training expenses. The qZSSRC topology is not the only possible option to be used in the Optiverter and other dc–dc converter topologies with comparable performance could be applied. Also, Optiverter design for a wide input voltage range could impose limitations on the efficiency. However, improvements are possible at light load with the cycle skipping modulation, and by use of the reconfigurable rectifiers at high dc voltage gain.

REFERENCES

[1] S. Kouro, J. I. Leon, D. Vinnikov, and L. G. Franquelo, "Grid-connected photovoltaic systems: An overview of recent research and emerging PV converter technology," *IEEE Ind. Electron. Mag.*, vol. 9, no. 1, pp. 47–61, Mar. 2015.
[2] M. Kasper, D. Bortis, and J. W. Kolar, "Classification and comparative evaluation of PV panel-integrated DC–DC converter concepts," *IEEE Trans. Power Electron.*, vol. 29, no. 5, pp. 2511–2526, May 2014.
[3] SolarEdge Fixed String Voltage, Concept of Operation, Sep. 2012. [Online]. Available: https://www.solaredge.com. Accessed on: Jan. 28, 2018

[4] E. Liivik, A. Chub, R. Kosenko, and D. Vinnikov, "Low-cost photovoltaic microinverter with ultra-wide MPPT voltage range," in *Proc. 6th Int. Conf. Clean Elect. Power*, Santa Margherita Ligure, Italy, 2017, pp. 46–52.
[5] J. K. Kaldellis *et al.*, "Temperature and wind speed impact on the efficiency of PV installations. Experience obtained from outdoor measurements in Greece," *Renewable Energy*, vol. 66, pp. 612–624, Jun. 2014.
[6] L. Linares, R. Erickson, S. MacAlpine, and M. Brandemuehl, "Improved energy capture in series string photovoltaics via smart distributed power electronics," in *Proc. Asia-Pacific Econ. Cooperation*, Washington, DC, USA, 2009, pp. 904–910.
[7] M. Fornage, "Method and apparatus for converting direct current to alternating current," U.S. Patent 7 796 412 B2, Sep. 14, 2010.
[8] H. Hu, S. Harb, N. Kutkut, I. Batarseh, and Z. J. Shen, "A review of power decoupling techniques for microinverters with three different decoupling capacitor locations in PV systems," *IEEE Trans. Power Electron.*, vol. 28, no. 6, pp. 2711–2726, Jun. 2013.
[9] S. B. Kjaer, J. K. Pedersen, and F. Blaabjerg, "A review of single-phase grid-connected inverters for photovoltaic modules," *IEEE Trans. Ind. Appl.*, vol. 41, no. 5, pp. 1292–1306, Sep./Oct. 2005.
[10] P. Garrity, "Solar photovoltaic power conditioning unit," U.S. Patent 8 391 031 B2, Mar. 05, 2013.
[11] SolarEdge P300/P370/P404/P405/P500/P505 Power Optimizer. [Online]. Available: http://www.solaredge.com. Accessed on: Jan. 28, 2018.
[12] Enphase M250 Microinverter Datasheet. [Online]. Available: https://enphase.com. Accessed on: Jan. 28, 2018.
[13] Enecsys 240-60-MP Microinverter Datasheet. [Online]. Available: http://manualzz.com.Accessed on: Jan. 28, 2018.
[14] D. Vinnikov, A. Chub, E. Liivik, and I. Roasto, "High-performance quasi-Z-source series resonant DC–DC converter for photovoltaic module-level power electronics applications," *IEEE Trans. Power Electron.*, vol. 32, no. 5, pp. 3634–3650, May 2017.
[15] T. LaBella, W. Yu, J. S. Lai, M. Senesky, and D. Anderson, "A bidirectional-switch-based wide-input range high-efficiency isolated resonant converter for photovoltaic applications," *IEEE Trans. Power Electron.*, vol. 29, no. 7, pp. 3473–3484, Jul. 2014.
[16] D. Vinnikov, A. Chub, E. Liivik, F. Blaabjerg, and S. Kouro, "Maximizing energy harvest of the impedance source PV microconverter under partial shading conditions," in *Proc. CPE-POWERENG*, Doha, Qatar, Apr. 10–12, 2018, pp. 1–7.
[17] D. Vinnikov, A. Chub, I. Roasto, and L. Liivik, "Multi-mode quasi-Z-source series resonant DC/DC converter for wide input voltage range applications," in *Proc. Asia-Pacific Econ. Cooperation*, Long Beach, CA, USA, 2016, pp. 2533–2539.
[18] F. C. Schwarz, "A method of resonant current pulse modulation for power converters," *IEEE Trans. Ind. Electron. Control Instrum.*, vol. IECI-17, no. 3, pp. 209–221, May 1970.
[19] J. E. Huber, J. Miniböck, and J. W. Kolar, "Generic derivation of dynamic model for half-cycle DCM series resonant converters," *IEEE Trans. Power Electron.*, vol. 33, no. 1, pp. 4–7, Jan. 2018.
[20] J. Park, M. Kim, and S. Choi, "Zero-current switching series loaded resonant converter insensitive to resonant component tolerance for battery charger," *IET Power Electron.*, vol. 7, no. 10, pp. 2517–2524, 2014.
[21] J. P. Vandelac and P. D. Ziogas, "A DC to DC PWM series resonant converter operated at resonant frequency," *IEEE Trans. Ind. Electron.*, vol. 35, no. 3, pp. 451–460, Aug. 1988.
[22] D. Vinnikov, T. Jalakas, I. Roasto, H. Agabus, and K. Tammet, "Method of shoot-through generation for modified sine wave Z-source, quasi-Z-source and trans-Z-source inverters," U.S. Patent 9 214 876 B2, Dec. 15, 2015.
[23] I. Roasto, D. Vinnikov, J. Zakis, and O. Husev, "New shoot-through control methods for qZSI-based DC/DC converters," *IEEE Trans. Ind. Informat.*, vol. 9, no. 2, pp. 640–647, May 2013.
[24] D. Vinnikov, I. Roasto, L. Liivik, and A. Blinov, "Four novel PWM shoot-through control methods for impedance source DC–DC converters," *J. Power Electron.*, vol. 15, no. 2, pp. 299–308, 2015.
[25] I. Roasto, D. Vinnikov, T. Jalakas, J. Zakis, and S. Ott, "Experimental study of shoot-through control methods for qZSI-based DC/DC converters," in *Proc. SPEEDAM*, Pisa, Italy, 2010, pp. 29–34.
[26] E.-H. Kim and B.-H. Kwon, "Zero-voltage- and zero-current-switching full-bridge converter with secondary resonance," *IEEE Trans. Ind. Electron.*, vol. 57, no. 3, pp. 1017–1025, Mar. 2010.
[27] L. Zhang, R. Born, X. Zhao, and J. S. Lai, "A high efficiency inverter design for Google little box challenge," in *Proc. Wide Bandgap Power Devices Appl.*, Blacksburg, VA, USA, 2015, pp. 319–322.
[28] O. Husev *et al.*, "Voltage distortion approach for output filter design for off-grid and grid-connected PWM inverters," *J. Power Electron.*, vol. 15, no. 1, pp. 288–297, Jan. 2015.
[29] R. Hasan, S. Mekhilef, M. Seyedmahmoudian, and B. Horan, "Grid-connected isolated PV microinverters: A review," *Renewable Sustain. Energy Rev.*, vol. 67, pp. 1065–1080, Jan. 2017.
[30] W. Bower, C. Whitaker, W. Erdman, M. Behnke, and M. Fitzgerald, "Performance test protocol for evaluating inverters used in grid-connected photovoltaic systems," CEC, Sacramento, CA, USA, Oct. 2004.
[31] S. Kapat, A. Patra, and S. Banerjee, "Achieving monotonic variation of spectral composition in DC–DC converters using pulse skipping modulation," *IEEE Trans. Circuits Syst. I, Reg. Papers*, vol. 58, no. 8, pp. 1958–1966, Aug. 2011.
[32] H. Hu, W. Al-Hoor, N. H. Kutkut, I. Batarseh, and Z. J. Shen, "Efficiency improvement of grid-tied inverters at low input power using pulse-skipping control strategy," *IEEE Trans. Power Electron.*, vol. 25, no. 12, pp. 3129–3138, Dec. 2010.
[33] K. Ishaque, Z. Salam, and Syafaruddin, "A comprehensive MATLAB Simulink PV system simulator with partial shading capability based on two-diode model," *Solar Energy*, vol. 85, no. 9, pp. 2217–2227, Sep. 2011.

Dmitri Vinnikov (M'07–SM'11) received the Dipl.Eng., M.Sc., and Dr.Sc.Techn. degrees in electrical engineering from the Tallinn University of Technology, Tallinn, Estonia, in 1999, 2001, and 2005, respectively.

He is currently the Head of the Power Electronics Group, Department of Electrical Power Engineering and Mechatronics, Tallinn University of Technology and a Guest Researcher with the Institute of Industrial Electronics and Electrical Engineering, Riga Technical University, Riga, Latvia. He is the Head of R&D and cofounder of Ubik Solutions LLC – Estonian start-up company dedicated to innovative & smart power electronics for renewable energy systems. Moreover, he is one of the founders and leading researchers of ZEBE – Estonian Centre of Excellence for zero energy and resource efficient smart buildings and districts. He has authored or coauthored two books, five monographs, and one book chapter, as well as more than 200 published papers on power converter design and development and is the holder of numerous patents and utility models in this field. His research interests include applied design of power electronic converters and control systems, renewable energy conversion systems (photovoltaic and wind), impedance-source power converters, and implementation of wide bandgap power semiconductors.

Andrii Chub (S'12–M'17) received the B.Sc. and M.Sc. degrees in electronic systems from the Chernihiv State Technological University, Chernihiv, Ukraine, in 2008 and 2009, respectively, and the Ph.D. degree in electrical engineering from the Tallinn University of Technology, Tallinn, Estonia, in 2016.

He is a Researcher with the Power Electronics Group, Tallinn University of Technology. He was a Visiting Research Fellow with Kiel University, Kiel, Germany, working in ERC project "Highly Efficient and Reliable Smart Transformer" between January and July 2017. He has coauthored more than 60 papers and a book chapter on power electronics and applications. He holds several patents and utility models. His research interests include advanced dc–dc and dc–ac converter topologies, impedance-source electric energy conversion technology, application of the wide bandgap semiconductors in power electronic converters, renewable energy conversion systems for energy efficient residential buildings, and converter topologies for smart transformers.

Elizaveta Liivik (S'12–M'16) received the Dipl.-Eng., M.Sc. and Ph.D. degrees in electrical engineering from the Department of Electrical Drives and Power Electronics, Tallinn University of Technology, Tallinn, Estonia, in 1998, 2000, and 2015, respectively.

She is currently a Researcher with the Department of Electrical Power Engineering and Mechatronics, Tallinn University of Technology. From 2002 to 2007, she was a lecturer with the Department of Electrical Drives and Power Electronics, Tallinn University of Technology. She has authored or coauthored more than 40 research papers and one book. Her research interests include impedance-source power electronic converters, renewable energy, and distributed generation, as well as control and reliability issues of power electronic converters in active distribution networks.

Roman Kosenko (S'14) received the Dipl.-Eng. and M.Sc. degrees in electronics from the Department of Industrial Electronics, Chernihiv State University of Technology, Chernihiv, Ukraine, in 2011 and 2013, respectively. He is currently working toward the Ph.D. degree in electrical engineering with the Department of Electrical Power Engineering and Mechatronics, Tallinn University of Technology, Tallinn, Estonia, and with the Biomedical Radioelectronic Apparatus and Systems Department, Chernihiv National University of Technology, Chernihiv, Ukraine.

He is author or coauthor of 14 scientific papers and is the holder of three utility models in the field of power electronics. His research interests include research, design, and simulation of switch mode converters for distributed power generation systems.

Oleksandr Korkh (S'16) received the B.Sc. and M.Sc. degrees in electronics from the Department of Industrial Electronics, Chernihiv National University of Technology, Chernihiv, Ukraine, in 2015 and 2017, respectively. He is currently working toward the Ph.D. degree in electrical engineering with the Department of Electrical Power Engineering and Mechatronics, Tallinn University of Technology, Tallinn, Estonia.

He is author or coauthor of several scientific papers. His research interests include the design, simulation, and control systems of converters for renewable power generation systems and storage systems in battery applications.